Optical/IR Interferometry: Concepts, Terminology, and the Current Status

Chris Haniff

Astrophysics Group, Cavendish Laboratory, University of Cambridge, JJ Thomson Avenue, Cambridge CB3 0HE, UK

Abstract.   The use of optical/infrared interferometric methods by non-interferometric specialists is becoming more commonplace, and offers many opportunities for novel studies at high angular resolution. This paper presents an overview of current optical/IR interferometric methods for non-experts, with particular emphasis on the basic terminology and concepts. It also outlines the capabilities of current and planned interferometers and reviews some recent science applications. The goals are to provide the background needed for a non-expert to assess the utility of interferometry for potential scientific studies and to help identify those capabilities of existing arrays that offer the best prospects for future science exploitation.

1. Introduction

The advent of "facility-class" ground-based optical and infrared (IR) interferometers such as ESO's Very Large Telescope Interferometer (VLTI) has led to an increasing body of literature reporting studies that have exploited interferometric methods at optical/IR wavelengths. However, unlike the situation in contemporary life, where new technologies are often adopted at an exponential rate through both enhanced individual usage and a fast-growing cohort of new users,[1] it is unclear whether the growing interferometric literature has been linked to an expansion of the technique's user base.

One school of thought is that the method itself is "complicated," and so only expert users can exploit it usefully, while others suggest that a perceived steep learning curve puts potential users off. Both of these are likely to be true at some level, and so this review aims to address the SOC's charge to the author:

> To introduce the non-specialists in the audience to optical interferometry terminology and concepts, and to give them a quantitative idea of the capabilities (e.g., spatial and spectral resolution, limiting sensitivity, image fidelity and dynamic range) of current and planned interferometers.

With this in mind, this paper comprises three principal parts. Section 2 focuses on the concepts and terminology of optical/infrared (OIR) interferometry at a level that should allow complete novices to assess the expert literature and follow many of the arguments presented. Section 3 highlights some of the more subtle and implementational difficulties that arise in practice; this will likely be of use to those who are planning

---

[1]For example, the use of cell phones, and social networking sites.

an interferometric experiment or assessing whether one might be feasible or valuable. Finally, section 4 presents a brief summary of the current state of the art and presents an overview of some of the science areas that have benefited from interferometric observations in the past few years.

In view of the SOC's request for me to focus on the non-experts in the audience, my presentation is deliberately non-mathematical. Much more information and detail, both on techniques and applications, can be found in the proceedings from two recent VLTI-focused schools (Malbet & Perrin 2007; Delplancke & Mosoni 2009). The enthusiastic reader is encouraged to review these two volumes for a much more comprehensive introduction to the subject than this brief summary can possibly deliver.

2.   Concepts and Terminology

2.1.   The Two-Element Adding Interferometer

The most important concepts of interferometry can be introduced using the example of a two-element adding interferometer, with the knowledge that a more complicated interferometric array can be thought of as simply replicating this basic structure in parallel many times. The key elements of such an instrument are shown in Figure 1.
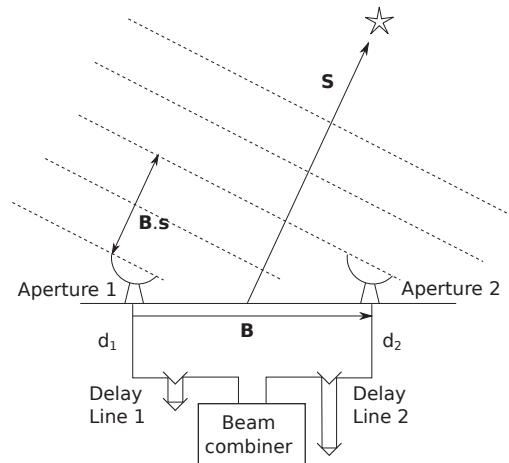

Figure 1.   Schematic cartoon of a two-element adding interferometer. The source is assumed to be unresolved and in the far-field, so that the wavefronts arriving at the ground are planar. The signals from each aperture or "unit telescope" are transported to a common beam combiner, having had their optical paths equalized using delay lines. They are then mixed, and the resulting combined signal is detected using a fast-readout, low-noise sensor; d_1 and d_2 refer to the optical paths from each antenna to the beam combiner.

From a functional perspective, such an interferometer *samples* the radiation from a target at two locations on the ground separated by some vector **B**: this is the *baseline* vector. The light is subsequently *transported* to a common location where the two signals are added together in a *beam combiner*,[2] and the resulting combined output is

_____

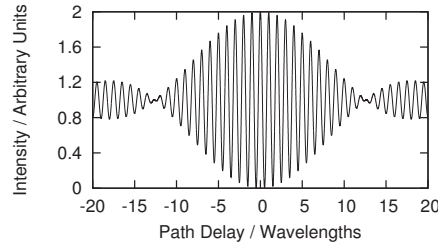[2]In radio astronomy this would be referred to as the correlator.

Figure 2.   The output of a polychromatic two-element adding interferometer as a function of the path delay between the interfering beams. The envelope function responsible for the difference between this and the expression in equation 1 arises from the assumption here of a non-zero fractional bandwidth, $\Delta\lambda/\lambda$, of roughly 8%.

detected. As can be seen from Figure 1, there will, in general, be a difference in the propagation lengths for any given wavefront to the two array elements, the magnitude of which will be given by the projection of the baseline vector in the pointing direction, **s**. This *geometric delay* (= **B**.**s**) is compensated for by introducing an equivalent delay into the propagation path from one of the array elements to the beam combiner using a device called a *delay line*. After this equalization of the optical paths, both beams will have travelled equal distances from the target to the component within the beam combiner where interference eventually occurs.

In comparison with the single dish measurements that most optical/IR astronomers will be used to, the most crucial distinctions in this scheme are the need for optical path equalization, and the fact that it is the detection of the summed signal, rather than the individual signals arriving at the two array elements, that is important.

2.2.   Interferometric Fringes

The response of a two-element interferometer, observing at wavelength λ, to a distant unresolved source is, in general, an intensity signal, I, that varies sinusoidally in the form

$$I \propto 1 + \cos(kD). \tag{1}$$

Here $D = [\mathbf{B}.\mathbf{s} + d_1 - d_2]$ and $k = 2\pi/\lambda$. The harmonic variation implied by equation 1 can be visualised at the detector in multiple ways, for example, by varying k, by altering d_1 or d_2, or by adjusting the baseline. All of these methods are used in practice, but regardless of the specifics of the implementation, the co-sinusoidally varying signature of such an interferometric output is what is universally referred to as the *fringe pattern*. In the polychromatic case in which a range of wavelengths, $\Delta\lambda$, is detected (Figure 2), the fringes are additionally modulated by a function related to the fractional bandwidth of the signal. This modulating function is referred to as the *coherence envelope*[3] and has a characteristic width in the order of *coherence length*, L_c (= $\lambda^2/\Delta\lambda$). For resolved targets, the output will be given by the superposition of a sequence of slightly non-overlapping polychromatic responses. Each of these can be thought of as originating

---

[3]Radio astronomers sometimes refer to this as the "delay beam." Note that the coherence envelope and the spectral bandpass form a Fourier transform pair.

Table 1.   Summary of common "derived" interferometric observables used in the OIR interferometric literature. The reader should note how the measurements of the Michelson visibility, *V*, and fringe phase, ϕ—both of which are real quantities derived from the intensity output of the interferometer—are combined to give the complex visibility and the complex bispectrum.

Name	Value	Description
Complex visibility	$Ve^{i\phi}$	Complex number combining Michelson visibility and fringe phase
V-squared	$V^2 = |Ve^{i\phi}|^2 = Ve^{+i\phi} \cdot Ve^{-i\phi}$	Square of the Michelson visibility
Differential phase	$\phi_{diff} = \phi_{\lambda_2} - \phi_{\lambda_1}$	Difference in fringe phase measured at two wavelengths
Closure phase	$\psi_{cp} = \phi_{12} + \phi_{23} + \phi_{31}$	Sum of fringe phases measured around a closed loop of baselines
Bispectrum (triple product)	$B_{123} = V_{12}\, e^{i\phi_{12}} V_{23}\, e^{i\phi_{23}} V_{31}\, e^{i\phi_{31}}$ $= V_{12}\, V_{23}\, V_{31}\, e^{i(\phi_{12}+\phi_{23}+\phi_{31})}$	Complex product of visibilities measured on a closed loop of baselines

from a spatially distinct infinitesimal element of the source brightness distribution, and will produce an output with a position-dependent fringe phase.

Three features of the interferometric output are of most interest, primarily because they tell the observer something about the source brightness distribution. These are

1. The *correlated flux*: the amount of signal contributing to the oscillating component of the interferometric output. This quantifies how much of the source flux is unresolved at an angular scale of λ/B_{proj}, where B_{proj} is the projected baseline length (see subsection 2.3).

2. The *fringe phase*: the location of the central fringe maximum relative to the zero optical path difference ($D = 0$) position on the detector. This measures the position of the target.

3. The *Michelson visibility*: the ratio of the total flux to the correlated flux. This is also given by $V = [I_{max} - I_{min}]/[I_{max} + I_{min}]$, where I_{max} and I_{min} correspond to the maximum and minimum detected intensities that would have been measured in the absence of the modulation provided by the coherence envelope.

Frequently these "raw" observables are presented in a "packaged" form with names such as *complex visibility*, *differential phase*, or *bispectrum*, and it is these derived quantities that one most often sees in the literature. A summary of these key interferometric observables is given in Table 1. What may be unclear to the novice is how the observables of Table 1 are related to what is likely of most interest to the observer, i.e., "What does the target look like?" The following subsection addresses this key question.

2.3. The van Cittert Zernike Theorem and the Fourier Plane

The fundamental basis for spatial interferometry is the van Cittert Zernike theorem which states that "the complex visibility is the Fourier transform of the source brightness distribution". In mathematical terms this is often presented as:

$$V(u, v) = \int I(\alpha, \beta) \exp\left(-i2\pi\left[\alpha u + \beta v\right]\right) d\alpha\, d\beta, \tag{2}$$

where $I(\alpha, \beta)$ is the source intensity at sky coordinates α and β, and $V(u, v)$ is the complex visibility function measured at *spatial frequencies u* and *v*. These coordinates are related to the mean observing wavelength and the projections of the baseline onto a plane perpendicular to the pointing direction as follows: $u = B_x/\lambda$ and $v = B_y/\lambda$. This plane is conventionally referred to as the (u, v) or *Fourier plane*, and any given projected interferometer baseline will map onto a point in this plane.[4] The reader should note that as the source position changes during the night, the projected baselines will change and so different spatial frequencies will be sampled by the interferometer. This time-varying sampling of the Fourier plane is known as *Earth rotation synthesis*.

Equation 2 implies that we can view an optical interferometer (indeed any interferometer) simply as a large machine for measuring the Fourier components of a source, i.e., the amplitudes and phases of the Fourier transform of the source brightness distribution. Furthermore, these measurements will be made at co-ordinates (u, v) in the Fourier plane that are directly related to the interferometer baselines. Short interferometer baselines will sample regions of the Fourier plane at low spatial frequencies, whereas long baselines will allow interrogation at high spatial frequencies.

The interferometric observables enumerated in Table 1 are thus connected to the source in the following ways. The *Michelson visibility* is the amplitude of the normalised Fourier transform of the source brightness distribution, while the *fringe phase* is its argument. When combined in the *complex visibility* they give a direct measurement of a single complex Fourier component of the image at a spatial frequency determined by instantaneous interferometer baseline. The *differential phase* and *closure phase* are linear combinations of the Fourier phases, while the *bispectrum* is a product of three complex visibilities where, for reasons to be explained later, the spatial frequencies at which the visibilities have been measured sum to zero. The merit of these linear combinations of Fourier phases is that they are to first order unperturbed by seeing fluctuations.

2.4. Exploiting Interferometric Data

In principle, if the Fourier transform of the source brightness distribution is measured well enough—by which we mean in a sufficiently dense, well-calibrated, and quasi-uniform manner—it is possible to invert the visibility function to recover an image. This is standard practice in radio and millimetre interferometry, but at optical/IR wave-

---

[4]In fact, because the source brightness distribution is a real function, it is usual to associate a given baseline with *two uv* points, one at (u, v) and the other at $(-u, -v)$ at which the value of $V(-u, -v)$ will be equal to the complex conjugate of that at $V(u, v)$.
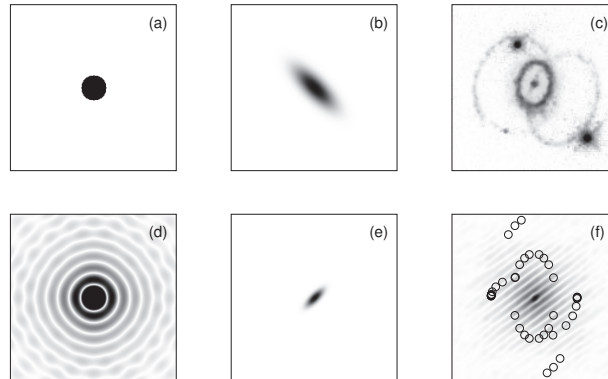
Figure 3.   Examples of three source intensity distributions (top row) and the amplitudes of their corresponding visibility functions (bottom row). Note how the sharp edge of the uniform disk, (a), gives rise to sidelobes in $V(u, v)$ that extend to high spatial frequencies, while the Gaussian profile of the elliptical source, (b), leads to a smooth, rapidly decaying visibility function, whose major axis is aligned along the most compact axis of the target. The most complex source (c) has a correspondingly complicated visibility function, with the two bright point-like features in the image producing the fringes seen in $V(u, v)$, and the remaining structure giving rise to more subtle variations in the visibility amplitude. The hollow circles in panel (f) show the sparse uv-plane coverage typical of a non-spectrally dispersed optical/IR observation. Sub-image (c) is reproduced courtesy of the STScI.

lengths, it is more usual to take the measured interferometric observables and use these as constraints in a model-fitting procedure.[5]

As a result, a key step in the planning of any OIR interferometric experiment is an assessment as to which Fourier components and interferometric observables are likely to be most useful in constraining the uncertainties in the source. With this in mind, it is helpful to spend a moment looking at some simple Fourier transform pairs. Figure 3 presents a sequence of sources of increasing complexity, together with the moduli of their Fourier transforms. The figure caption highlights some of the key features of these transform pairs, but three additional points are worth stressing:

- Localized structures in the source give rise to distributed features in the visibility function, and so measurements of a single uv datum are rarely sufficient to provide useful insights unless the source is already very well constrained.

- The visibility function peaks at the origin and, for most source morphologies, presents considerably lower values at higher spatial frequencies.

_____

[5]The reasons for this are broadly speaking twofold: first, it is usually very time consuming to secure a sufficiently large number of uv-plane data, and second, the atmospheric perturbations present at optical/IR wavelengths mean that it is usually not as straightforward to invert the Fourier data as it is at wavelengths where the atmosphere is more benign.

Table 2.　　Summary of common methods used to exploit OIR interferometric observables for astronomy. In each case the brief description indicates what quantities are measured and how these can lead to a better understanding of the science target.

"Mode"	Description
Astrometry	Measure geometric delay for a range of different targets. Uses measurements of ϕ. Determines separations projected along the baseline orientation through differences in the phases.
Nulling	Introduces a deliberate delay in one arm of the interferometer to give no response for an on-axis source. An off-axis planet can be detected through the small signal that leaks through.
V^2 science	Measure V^2 for a range of projected baselines. Fit a model of the source to these data. Is unable to identify source asymmetries, for which phase information is required.
Closure phase/differential phase science	Measure ϕ_{diff} or ψ_{cp} for a range of projected baselines. Optionally combine with V^2 data and then model-fit as for V^2. Large enough sets of $\{V^2, \phi_{diff}, \psi_{cp}\}$ can provide very strong constraints on possible source structure.
Imaging	Combine multiple V^2, and some mix of closure phase, differential phase and true phase data, and invert. Strongly dependent on quality and completeness of dataset.

- The low signal typical at high spatial frequencies means that in general, measurements of the visibility function at these locations—which glean information about the small scale structure of the source—will be difficult to make.

The first and last of these points are, at some level, in conflict, and so it should not be a surprise that the majority of OIR interferometric studies have not generated detailed high resolution maps of their targets of interest, but rather have capitalized on using the interferometric observables as model-dependent diagnostics. A summary of these methods is given in Table 2. This sequence reveals a hierarchy, where as one continues down the table eventually one has assembled enough visibility amplitude and phase information that the type of model-independent imaging commonplace at radio wavelengths becomes possible.

A number of important features of a typical OIR interferometric observation are captured in the lower right-hand panel of Figure 3. This shows the visibility amplitudes for a complex source, together with symbols that represent the projected baseline coordinates for an interferometer at the times at which its measurements are assumed to have been made. These hollow circles show the locations at which the visibility function has been measured, and one can see that these have traced out elliptical arcs as a result of Earth rotation. The three *uv tracks* are indicative of the use of a three-element array, for which there are three instantaneous baselines. In addition, the discrete nature of the tracks, i.e., they are not continuous, reflects the fact that it can take up to 30 minutes to secure enough fringe data to allow the value of the visibility function to be measured reliably at a single *uv*-plane coordinate.

Although such sparse sampling of the *uv*-plane would not be adequate to recover an image, a time series of the V^2 data on the intermediate length baseline would reveal the oscillating signature of the angled fringes seen in the visibility function. This would not only detect the presence of the two point sources in the target but would also allow their separation, fluxes, and orientation on the sky to be measured. For unequal components, a closure phase measurement would then straightforwardly establish the parity of the pair, i.e., which was located to the South and which to the North.

3.   Difficulties and Shortcomings

Although the previous conceptual description of interferometry has been relatively straightforward, there are a number of subtleties of the method that may be unfamiliar to newcomers to the field. The most important of these have been outlined below and have been separated into those that are intrinsic to the method and those that are specific to the optical/IR regime. Because of space limitations, it has not been possible to do much more than list these features of the method, but I hope this brief presentation is still useful enough to point the inquisitive reader in the right direction when searching the literature.

3.1.   Generic Limitations of Interferometry

3.1.1.   Fourier Plane Sampling.   Previous sub-sections have already mentioned the need for good Fourier plane sampling. This is never an issue with a conventional telescope, which is sensitive to all spatial frequencies from zero up to D/λ (D is the telescope diameter). However, since interferometers must sample the *uv*-plane discretely, this is a major consideration when planning any interferometric experiment. In all cases the number of independent samples of the visibility function should be greater than the number of degrees of freedom in the model being fitted (or the number of image pixels to be recovered). In addition, for imaging studies, the *uv* coverage should be as uniform as possible.

It is essential for the newcomer to realize that any given interferometric observation will only be sensitive to structures on angular scales of $\theta \sim \lambda/B_{proj}$, and so if an experiment is to determine the structure of an unknown target with some angular resolution, θ_{res}, then it is desirable that measurements of the visibility function be made for projected baselines ranging from the *zero spacing*, i.e., where $u = v = 0$, to λ/θ_{res}. More importantly, if the ratio of the longest to the shortest interferometer baseline used is R, then this will also be equal to the ratio of the highest and lowest angular scales the observation will be sensitive to. As well as moderating an experiment's sensitivity to different angular scales, the *uv*-plane sampling will also have an impact on the dynamic range of any synthesized image. In the case of quasi-uniform sampling of the Fourier plane, the dynamic range will be given roughly by the product of the signal-to-noise ratio per Fourier datum and the square root of the number of *uv* data measured.

The impact of these well-established rules of thumb cannot be overestimated. In a typical optical/IR experiment, the ratio of maximum to minimum baseline length rarely exceeds 10, and the total number of independent samples of the visibility function is usually less than 100. As a result, the delivery of even a 10×10 pixel image with a dynamic range of 100:1 remains a significant challenge. This has been achieved in a small number of cases, but more usually the sparsely sampled interferometric data

are combined with other data, such as spectral energy distributions, and used in multi-parameter model-fitting schemes instead.

3.1.2.   Spectral Resolution and Field of View.   The maximum permissible bandpass for any interferometric measurement will in general be set by the coherence length of the light being interfered, and so for broadband studies, spectral dispersion of the bandpass is obligatory. For example, in the near-IR *K* band, it is usual to operate with a spectral resolution, R (= $\lambda/\Delta\lambda$) of at least 30, i.e., with roughly five spectral channels across the band.

The spectral resolution is also related to the maximum field of view for an interferometric observation. More specifically, the field of view will, apart from a few special cases, be given by the product of the spectral and spatial resolution, i.e., FOV $\approx$ $(\lambda/\Delta\lambda) \times (\lambda/B_{max})$. This will usually be considerably smaller than is usual for other high angular resolution optical/imaging studies. For example, for a typical low spectral resolution VLTI observation at $2.2\,\mu$m, the interferometric field of view will be no more than roughly $0.5''$. This is consistent with the typical minimum baselines available at separated-element arrays (of order $10\,$m), which limit the largest scales an interferometer is sensitive to, no more than $\sim \lambda/B_{min}$. The reader should note that this interferometric limitation to the field of view is completely independent of the more practical difficulty of propagating a large optical field of view to a beam combiner that may be located several hundred metres away from the array elements.

3.1.3.   Integration Time.   We have already mentioned the role of Earth rotation in allowing a fixed configuration of array elements to sample different locations in the *uv*-plane during a long observation of a target. This benefit, however, has a downside in that there will be a maximum integration time for any measurement at a given spatial frequency, beyond which time the Earth will have rotated enough that a new independent Fourier component will have begun being measured. For a source with maximum extent θ_{max}, spatial frequencies separated by more than $\Delta u \approx 1/\theta_{max}$ will provide independent information on the target. For most optical/IR experiments this corresponds to roughly 5–10 minutes of Earth rotation, and so if longer observation times are needed to build up enough signal-to-noise at a single *uv*-datum, then data taken at appropriate times on different nights must be co-added.

3.1.4.   Calibration.   A final important aspect of all interferometric investigations is the need to carefully calibrate the interferometric observables. Although we have described the Michelson visibility and fringe phases as being unambiguous metrics for the Fourier components of the source brightness distribution, there are numerous instrumental effects that can alter the measured observables from their true values. In a sense we should view them as particularly "fragile" observables. For example, if the beam paths from two telescopes to the beam combiner do not have equal transmission functions, this will lead to a systematic error in the measured Michelson visibility. The precise causes of such calibration errors need not concern us here, but, whatever their origin, it is standard practice to intersperse interferometric observations of a science target with measurements of one or more *calibrators*, i.e., targets for which the Fourier amplitudes and phases are known. These are usually chosen to be unresolved sources for which the visibility amplitudes and phases are unity and zero, respectively, for all of the interferometer baselines. Alternatively, it may be easier to use partially resolved stars with featureless and circularly symmetric photospheres whose diameters are al-

ready known, but which may be closer in angle on the sky and in brightness to the science target.

The frequency with which such calibration observations must be secured varies from array to array, but there is general agreement that the reliability of most, if not all, OIR interferometric studies have been limited by calibration as opposed to random error. Science observations are thus almost always prefaced and followed by calibration measurements that take as much time to secure as the science data itself. The consequent reduction in duty-cycle is thus the price that has to be paid to ensure that the interferometric data will be of scientific use.

3.2. Limitations Specific to the Optical/IR Domain

Before moving onto the final part of my presentation, it will be useful to outline a number of key differences between the implementation of interferometry at optical/IR wavelengths and what is more usual in the radio and mm/sub-mm domain. We have mentioned one or two of these divergences already in passing, but it will be helpful for novices to see these reviewed again so that these differences are properly understood.

3.2.1. Amplification and its Implications. One of the most important differences between interferometry at optical/IR and radio wavelengths is the lack of useful amplification.[6] This has manifold repercussions, including, not only a limitation on the faintest targets that can be observed, but also a constraint on how many ways the signal from an individual array element can be split and combined with that from other array elements. Because of this, it is usual for optical/IR beam combiners to combine no more than 2–6 beams simultaneously to as to optimize the overall signal-to-noise.

An N-beam correlator can provide up to $N(N-1)/2$ different baselines, and so this limit strongly impacts how rapidly large datasets of Fourier data can be secured in comparison with the radio. For example, the correlator at the EVLA has been designed to accommodate signals from 32 telescopes at once, giving 496 measurements of the visibility function simultaneously. By way of comparison, a typical three-way infrared beam combiner, such as the common user AMBER instrument at the VLTI, will be two orders of magnitude slower in accessing the *uv*-plane.

3.2.2. Atmospheric Perturbations. The second most important difference between centimetric radio interferometry and its optical/IR implementation is the impact of the atmosphere. The atmospheric perturbations—which optical astronomers will recognize as the *seeing*—can be thought of as primarily altering the phases of the wavefronts arriving from a source. An initially planar wavefront, having entered the atmosphere, will, by the time it reaches the ground plane, exhibit random corrugations due to differences in the refractive index of the air along the paths taken by different rays from the source to the ground. The strength of the atmospheric perturbations is usually characterized by two physical scales, one spatial and one temporal, and it is the magnitudes of these with respect to the operating parameters of the array that are very different in the optical/IR and radio.

The strength of the spatial perturbations is characterized by a linear scale—more commonly referred to as *Fried's parameter* or r_0—which can be thought of as the radius

---

[6]Here we mean amplification so as to not decrease the overall signal-to-noise ratio. This is a fundamental limitation associated with quantum uncertainty, not merely a technological constraint.
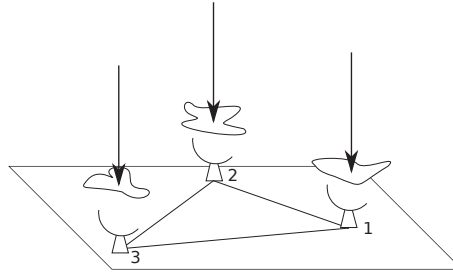
Figure 4. A cartoon showing the impact of refractive index fluctuations for a three-element array. For each baseline, ij, the measured Fourier phase, $\hat{\phi}_{ij}$, will be given by $\phi_{ij} + \epsilon_i - \epsilon_j$, where ϵ_i and ϵ_j are the phase errors associated with the refractive index perturbations along the lines of sight to the target from telescopes i and j. Implicit in the diagram is the assumption that a single number can characterize the phase errors for an individual antenna, which are shown schematically as the "clouds" above each telescope. If the measured Fourier phases are summed round a closed loop of baselines, in this case baselines 12, 23 and 31, this value will be independent of the antenna-based errors ϵ_1, ϵ_2, and ϵ_3. The sum $\phi_{12} + \phi_{23} + \phi_{31}$ is known as the closure phase ψ_{123}.

of a circular patch of the wavefront over which the rms. wavefront error is 1 radian. The value of Fried's parameter scales with wavelength as $\lambda^{6/5}$, and a good optical site will have a value for r_0 of around 15 cm at 500 nm. This can be compared to values of tens of km at centimetric radio wavelengths where r_0 is always much greater than the array collector size, and is usually comparable to the longest baseline length.

The impact of these spatial perturbations on the wavefronts sampled by the interferometer is threefold: first the measured correlated flux (and hence Michelson visibility) will be reduced; second, there will be an increased level of measurement fluctuation; and, third, the fringe phase will be altered from its "true" value. As a result, the presence of these spatial perturbations is a major limitation for ground-based OIR interferometry and makes the use of large telescopes as array elements problematic. All arrays use low-order (i.e., tip-tilt) systems to increase the effective r_0 values at their sites, and arrays that use 10 m-class telescopes, such as the Keck and VLT interferometers, are obliged to use *adaptive optics* (AO) systems to flatten the incoming wavefronts at the telescope apertures so as to exploit these larger dishes effectively. Nevertheless, even in these cases, the effective areas of the large unit telescopes are limited by the Strehl ratios that the AO systems can deliver.

An additional strategy is to *spatially filter* the beams from each array collector with a pinhole or piece of optical fibre. This has the effect of removing that part of the signal associated with the wavefront corrugations, and so trades off a loss in overall signal with a more reliable measurement of the correlated flux.

Unfortunately, the temporal fluctuations in the atmosphere are even more constraining. These are characterized by a temporal scale—the *coherence time*, t_0—that has a very similar definition to that of r_0; t_0 measures the time over which the rms. wavefront fluctuation at a fixed point on the ground is equal to 1 radian, and like r_0 scales as $\lambda^{6/5}$. A typical value for t_0 is 10 ms at 500 nm, and again this can be compared with the much larger values of several minutes that are typical of centimetric radio wavelengths.

The impact of these temporal fluctuations on interferometric observations will be threefold. First, they require that measurements of the interferometric output must be

secured on a timescale less than t_0. Longer integrations will give systematically reduced correlated fluxes, and fringe phases that are averaged over the exposure time, so that the raw interferometric observables will no longer be source-dependent alone. Second, the position of the delay lines needed to equalize the optical path will no longer be determined by geometry alone. Instead, it will be necessary to *search* and *track* the zero OPD position. Finally, even if instantaneous measurements are made at high signal-to-noise, the measured fringe phases will be corrupted by unknown *antenna-based* path length errors (see Figure 4) unless these have been monitored and been corrected for by precisely re-positioning the interferometer's delay lines in real-time.

Multiple strategies for mitigating the effects of these temporal fluctuations exist. Active approaches—which, broadly speaking, correspond to AO on the scale of the array—are now implemented in some form at all interferometers. The most common of these is called *coherencing* and refers to tracking the atmosphere fluctuations such that any residual atmospheric path errors are much less than the coherence length. More precise tracking, such that the errors are reduced to much less than a wavelength, is referred to as *phase tracking*. In certain, less-frequent cases this tracking can be performed relative to a fixed target in which case the measured fringe phases will become accurate proxies for the visibility phase. This is known as *phase referencing*.[7] Phase tracking and phase referencing can be undertaken using either the target itself or an off-axis guide star—whichever is used must not be significantly resolved on the baselines being tracked—but as in AO, issues such as the extent to which an off-axis reference correctly senses the on-axis perturbations, mean that the sky coverage of suitable reference stars is very small (i.e., typically less than 1%). Nevertheless, the benefits of these methods are considerable, and so for targets that are themselves suitably bright or have suitable reference stars, it can allow coherent integration of the interferometric signal for many seconds, giving more than a hundred-fold enhancement in the effective integration time.

These active methods are almost always used in parallel with passive techniques that capitalise on observables that are robust to the perturbations themselves. The two most common are the *differential phase* and the *closure phase*. The former is simply the difference in fringe phases measured at two wavelengths and is usually employed where the target can be assumed to be unresolved at one of these. In this case, because the chromatic behavior of the atmospheric perturbations is well understood, the differential phase is a proxy for the true visibility phase at the non-reference wavelength. The closure phase is the sum of the fringe phases around a closed loop of three baselines (see Figure 4) and is similarly immune to the atmospheric errors to first order. Measurement of the closure phase requires a three-element interferometer, but unlike the differential phase, its use makes no assumptions on the structure of the target at all, and so it is particularly useful for investigating targets that are expected to show complex structure on small angular scales. Because the closure phase is the argument of the product of the complex visibilities on the baselines comprising its closed loop, frequent mention is made of this *triple product*, which is also known as the *bispectrum*.

---

[7]The PRIMA and ASTRA systems at the VLTI and Keck implement this. A core feature of these systems is the presence of duplicated delay lines and beam combiners, one set of which is used for monitoring the atmosphere via the reference, with the other set receiving corrections from its partner and being tasked with the science observation.

Methods for best exploiting differential and closure phases for optical/IR studies are the subject of on-going research, but have been guided by experience of radio astronomical self-calibration techniques. Broadly speaking, these *good observables* are used either as constraints in model-fitting procedures or as inputs to iterative image reconstruction schemes that seek to determine an image that fits the measured Fourier data and is consistent with any other information about the target's structure and extent.

3.2.3.   Sensitivity.   Before reviewing the current status and prospects for OIR interferometry, it will be helpful to say a few words on the topic of sensitivity. This involves the same type of assessment as for an adaptive optics experiment in that the bottom line will be to ensure that one can detect and correct for the atmospheric perturbations. If this is possible, then a secondary question will be whether one can secure enough Fourier data with a sufficiently high signal-to-noise in the time available. For experiments that rely on sensing the atmosphere with a natural source, it is reasonable to expect a sensitivity comparable to that of natural guide star AO systems in the high Strehl limit. That is, it should be possible to secure observations in the near-IR *K* band at magnitudes of order 13. The use of laser guide stars would be expected to improve this considerably, although most laser guide stars will be far too extended to be useful for fringe tracking, and so their benefit is primarily in allowing larger-unit telescopes to be exploited as opposed to lengthening the effective exposure time.

If enough *uv*-plane data can be secured, then it is reasonable to expect that a dynamic range of order 100:1 should be routinely available. However, this may be limited by calibration errors. Such dynamic ranges have already been achieved in practice, but sensitivities comparable to those of natural guide star AO systems are still some way from being realized.

4.   Current Status and Prospects

A brief commentary on the status and prospects for OIR interferometry that focuses on programatics and funding occurs elsewhere in this volume (Ridgway 2011), and so in this concluding section I shall focus primarily on technical and scientific results. Further details of many of the interferometers and instruments mentioned below can be found in Malbet & Perrin (2007) and Delplancke & Mosoni (2009) and within the many papers presented at the SPIE San Diego biennial meeting on optical and infrared interferometry in 2010 (Danchi et al. 2010).

4.1.   Technical Status

The overall health of OIR astrophysics can be judged, in some sense, by the rate at which refereed scientific publications now appear. This rate is comparable to that of the early days of radio astronomy, albeit delayed by 32 years, and there is little evidence that this increasing trend is set to stop. The bulk of the most recent few years' papers report on data secured at the VLTI and CHARA arrays, but there are still a modest number of PI-class instruments elsewhere that continue to produce very useful and exciting science. A summary of the these is presented in Table 3 below, where brief details of their features and capabilities have been listed.

The range of capabilities summarized in Table 3 confirms that there is considerable activity worldwide. At the VLTI, two-beam combiners continue to provide common-user capabilities with spectral resolutions from 35 to 12000 in the near-IR (AMBER)

Table 3. Basic capabilities and features of a number of modern optical/IR interferometric arrays. The baseline ranges specified are those whose use has been reported in the literature: other longer baselines may exist but may not have been commissioned yet. Arrays with "astrometry" listed in the right-hand column have the subsystems, e.g., differential delay lines and suitable non-common path metrology, so to permit micro-arcsecond narrow-angle astrometry. The data for the MROI are design goals.

Name and location	Tel. size and baselines	Primary wavelength bands	Beam combiners
VLTI Paranal, Chile	4×8 m, 4×1.8 m 10–130 m	JHK and N	3-way $(J)HK$ Astrometry 2-way N
SUSI Narrabri, Australia	2×0.15 m 5–150 m	RI	2-way Astrometry
NPOI Flagstaff, AZ	6×0.12 m 7–98 m	RI	4-way Astrometry
CHARA Mt. Wilson, CA	6×1 m 31-331 m	RI and HK	6-way HK 3-way RI
KI Mauna Kea, HA	2 m 85 m	K and N	2-way Astrometry
ISI Mt. Wilson, CA	3×1.8 m 4–59 m	N	3-way
MROI Magdalena Ridge, NM	10×1.4 m 8–345 m	RI and JHK	Multiple 4-way systems

and from 30 to 230 in the mid-IR (MIDI). The current best sensitivities achieved are around $m_K \sim 7$ and $m_N \sim 6$, but these are expected to improve when the fringe trackers associated with the PRIMA astrometric instrument are commissioned in the near future. PIONIER, an integrated optics near-IR four-way visitor combiner, has also been used successfully there, and in addition two further second-generation instruments are in various stages of development: GRAVITY, a K band astrometric/imaging combiner that has been designed with a strong Galactic Center science focus, and MATISSE, a four-way combiner upgrade for MIDI.

In contrast, the SUSI and NPOI arrays share the use of small, approximately r_0-diameter collectors in the visible R and I bands, and have the potential to exploit very long baselines (up to 640 m at SUSI). Both have plans for micro-arcsecond astrometry—SUSI will use a new instrument, MUSCA—and have demonstrated very similar limiting sensitivities of around $m_R \sim 6$. Plans for an upgrade for the NPOI combiner are also in progress; their VISION instrument will permit six-way combination and offer spectral resolutions from 200 to 20000. The option of integrating much larger 1.8 m collectors into the NPOI remains a possibility, but the details of this are still in an embryonic phase.

The CHARA array continues to be the most prolific interferometric array in the US. It allows for V^2, differential phase, and closure phase measurement, and has operated at both visible and near-IR wavelengths. Its policy of encouraging visitor instruments has meant that a very large number of different beam combiners have been made available there. These have ranged from two-way K band bulk optics and fibre beam combiners, through the six-beam MIRC near-IR combiner, to the VEGA and PAVO optical instruments, the second of which is a copy of one of SUSI's correlators. Its best sensitivity in the near-IR has been at the $m_K \sim 8$ level for two-way combination but is a few magnitudes fainter for the MIRC instrument. Its visible (R) sensitivity limit is the range 7–8, depending on the spectral resolution chosen.

The Keck interferometer has successfully demonstrated both high sensitivity K band measurements down to $m_K \sim 11$ and a valuable nulling capability at 10 microns. It has offered a V^2 capability in the near-IR HKL bands and is currently being fitted with an astrometric instrument, ASTRA, whose goal will be to deliver 30 micro-arcsecond astrometry of targets close to the Galactic Center. This will capitalize on the facility laser guide star AO systems at each of the Keck telescopes so as to further enhance the limiting sensitivity of the array.

The final entry listed in Table 3 is for the Infrared Spatial Interferometer, which occupies a unique region of parameter space. This three-element array operates at around 11 microns and, unlike the other arrays described, operates in a *heterodyne* mode. Here the beams from each telescope are mixed with a coherent local oscillator, a CO_2 laser, and *down-converted* prior to being combined. This is identical to a radio interferometer, and this alternative scheme allows for very high spectral resolution ($> 10^6$) observations as well as more conventional V^2 and closure-phase measurements.

As well as this large complement of interferometric telescopes, there are many others tracers that indicate an active community. Extensive common-user observation preparation tools (ASPRO and getCal) have been developed on either side of the Atlantic, as have multiple reconstruction codes (e.g., MACIM, SQUEEZE and WISARD) for imaging from bispectrum and visibility amplitude data. In addition, there is an agreed optical interferometry standard (OIFITS) for exchanging calibrated data from different arrays that has been very successful in supporting OIR observables (see Table 1) that are not included in standard radio astronomical formats.

4.2. Recent Science Results

Perhaps more importantly, the scientific results from the arrays listed above have been both prolific and broad. Space permits only the most cursory of listings here, but these investigations have ranged from studies of the dust sublimation regions in active galactic nuclei (Kishimoto et al. 2011), through the detection of faint ($\Delta m \simeq 5$) companions to main sequence stars (Duvert et al. 2010), to the precision measurement of stellar radii and masses (Bazot et al. 2011) via a combination of interferometry and asteroseismology. High spectral resolution measurements of MWC 297 across the Br γ line have been reported by Weigelt et al. (2011), and in a number of studies, sufficient Fourier data has been secured to allow model-independent imaging.

Ultra-high angular resolution imaging has been a major success for the CHARA array, which has capitalized on its six 1 m-diameter telescopes and its multi-way near-IR beam combiner. Its ability to combine four (and most recently six) telescopes together simultaneously has given it a unique advantage in the near-IR. As well as a series of imaging studies of rapid rotators (see, e.g., Aufdenberg et al. 2006; Monnier et al.

2007) CHARA has also been responsible for allowing an exquisite set of infrared images of the transiting disk system in ϵ Aurigae (Kloppenborg et al. 2010) to be secured. These have solved the long standing controversy of the cause of its eclipses and directly confirmed the preferred model of a tilted disk of material that is geometrically thin but optically thick and in front of the 0.002″ diameter stellar disk. This quality of imaging has yet to be delivered by other arrays, but it clearly demonstrates what is already possible with a modest PI-scale instrument.

4.3.   Prospects for the Future

The next steps for ground-based optical/IR interferometry will clearly be a shift to a new paradigm in which model-independent imaging of faint targets becomes routine. This will leverage the effective collaborations between instrument builders, observers, and theoreticians that have arisen in the past few years but will require at least two significant developments at either augmented existing arrays or new facilities:

- A new generation of beam combiners that can accommodate beams from 4–6 telescopes simultaneously with high throughput and a spectrally dispersed capability.

- Enhanced sensitivity, by factors of 10–100, so as to close the gap between what has been achieved to date and what is needed for a broad science portfolio.

Instruments such as PRIMA, ASTRA, and GRAVITY, which have been designed to offer a phase-referencing capability, and which will be coupled with the use of large collectors (i.e., 2 m–10 m diameter) and adaptive optics, represent one approach to this evolution. These should be coming on line over the course of the next few years and will guarantee an enhanced capability for astrometry, imaging and V^2 science.

In parallel, 3rd-generation arrays will capitalise on the lessons learned at prototype and second-generation implementations. They have been designed to exploit new technologies, e.g., avalanche photo-diode arrays, that have only recently come about through initiatives for AO for the next generation of single-dish telescopes.

The Magdalena Ridge Observatory Interferometer—see Table 3 and Creech-Eakman et al. (2010)—is the best example of such a third-generation implementation. Located overlooking the VLA site in southern New Mexico, this 10-element facility will use 1.4 m diameter telescopes and exploit parallel switchable fringe-tracking and science beam combiners. It has been designed with high throughput and a high level of automation in mind, and will offer scalable Y-shaped telescope configurations with baselines ranging from 8 m to 345 m. Furthermore, it will support observations in both the optical and near-IR through use of vacuum beam relay and delay-line systems.

The broad high-level goals for either of these approaches will be a 50-fold enhancement in sensitivity, routine model-independent imaging, and a duty-cycle (for collecting of order 100 independent *uv* data) some 20–100 times better than has been achieved to date. These are challenging goals, but at present there appear to be no technical showstoppers to hinder this enterprise.

However, elsewhere in this volume Ridgway suggests that the vagaries of funding and other such considerations may make this path forward a time consuming and/or an unsteady one. My hope is that the recent successes touched on in this review promote a spirit of discovery and encourage a wider, ambitious community to seek a new view of the Universe with the new eyes that OIR interferometry is now offering.

References

Aufdenberg, J. P., Mérand, A., Coudé du Foresto, V., Absil, O., Di Folco, E., Kervella, P., Ridgway, S. T., Berger, D. H., ten Brummelaar, T. A., McAlister, H. A., Sturmann, J., Sturmann, L., & Turner, N. H. 2006, ApJ, 645, 664. arXiv:astro-ph/0603327

Bazot, M., Ireland, M. J., Huber, D., Bedding, T. R., Broomhall, A.-M., Campante, T. L., Carfantan, H., Chaplin, W. J., Elsworth, Y., Meléndez, J., Petit, P., Théado, S., van Grootel, V., Arentoft, T., Asplund, M., Castro, M., Christensen-Dalsgaard, J., Do Nascimento, J. D., Dintrans, B., Dumusque, X., Kjeldsen, H., McAlister, H. A., Metcalfe, T. S., Monteiro, M. J. P. F. G., Santos, N. C., Sousa, S., Sturmann, J., Sturmann, L., Ten Brummelaar, T. A., Turner, N., & Vauclair, S. 2011, A&A, 526, L4+

Creech-Eakman, M. J., Romero, V., Payne, I., Haniff, C., Buscher, D., Aitken, C., Anderson, C., Bakker, E., Coleman, T., Dahl, C., Farris, A., Jiminez, S., Jurgenson, C., King, R., Klingesmith, D., III, McCord, K., McCracken, T., Nyland, K., Olivares, A., Richmond, M., Romero, M., Salcido, C., Sandoval, J., Santoro, F., Seamons, J., Selina, R., Shtromberg, A., Steenson, J., Torres, N., Westpfahl, D., Baron, F., Fisher, M., Seneta, E., Sun, X., Wilson, D., & Young, J. 2010, in Society of Photo-Optical Instrumentation Engineers (SPIE) Conference Series, vol. 7734 of Society of Photo-Optical Instrumentation Engineers (SPIE) Conference Series

Danchi, W. C., Delplancke, F., & Rajagopal, J. K. (eds.) 2010, Optical and Infrared Interferometry II, vol. 7734 of Proc. SPIE (SPIE)

Delplancke, F., & Mosoni, L. 2009, NewAR, 53, 277

Duvert, G., Chelli, A., Malbet, F., & Kern, P. 2010, A&A, 509, A66+. 1001.5010

Kishimoto, M., Hönig, S. F., Antonucci, R., Barvainis, R., Kotani, T., Tristram, K. R. W., Weigelt, G., & Levin, K. 2011, A&A, 527, A121+. 1012.5359

Kloppenborg, B., Stencel, R., Monnier, J. D., Schaefer, G., Zhao, M., Baron, F., McAlister, H., Ten Brummelaar, T., Che, X., Farrington, C., Pedretti, E., Sallave-Goldfinger, P. J., Sturmann, J., Sturmann, L., Thureau, N., Turner, N., & Carroll, S. M. 2010, Nat, 464, 870. 1004.2464

Malbet, F., & Perrin, G. 2007, NewAR, 51, 563

Monnier, J. D., Zhao, M., Pedretti, E., Thureau, N., Ireland, M., Muirhead, P., Berger, J.-P., Millan-Gabet, R., Van Belle, G., ten Brummelaar, T., McAlister, H., Ridgway, S., Turner, N., Sturmann, L., Sturmann, J., & Berger, D. 2007, Science, 317, 342. 0706.0867

Weigelt, G., Grinin, V. P., Groh, J. H., Hofmann, K.-H., Kraus, S., Miroshnichenko, A. S., Schertl, D., Tambovtseva, L. V., Benisty, M., Driebe, T., Lagarde, S., Malbet, F., Meilland, A., Petrov, R., & Tatulli, E. 2011, A&A, 527, A103+. 1101.3695